



HAL
open science

**Research on Efficient Fast Scintillators: Evidence and
X-Ray Absorption Near Edge Spectroscopy
Characterization of Ce 4+ in Ce 3+ , Mg 2+ -Co-Doped
Gd 3 Al 2 Ga 3 O 12 Garnet Crystal**

Géraldine Dantelle, Georges Boulon, Yannick Guyot, Denis Testemale,
Malgorzata Guzik, Shunsuke Kurosawa, Kei Kamada, Akira Yoshikawa

► **To cite this version:**

Géraldine Dantelle, Georges Boulon, Yannick Guyot, Denis Testemale, Malgorzata Guzik, et al..
Research on Efficient Fast Scintillators: Evidence and X-Ray Absorption Near Edge Spectroscopy
Characterization of Ce 4+ in Ce 3+ , Mg 2+ -Co-Doped Gd 3 Al 2 Ga 3 O 12 Garnet Crystal.
physica status solidi (b), 2020, 257 (8), pp.1900510. 10.1002/pssb.201900510 . hal-02508822

HAL Id: hal-02508822

<https://hal.science/hal-02508822>

Submitted on 3 Nov 2020

HAL is a multi-disciplinary open access archive for the deposit and dissemination of scientific research documents, whether they are published or not. The documents may come from teaching and research institutions in France or abroad, or from public or private research centers.

L'archive ouverte pluridisciplinaire **HAL**, est destinée au dépôt et à la diffusion de documents scientifiques de niveau recherche, publiés ou non, émanant des établissements d'enseignement et de recherche français ou étrangers, des laboratoires publics ou privés.

**Research of efficient fast scintillators.
Evidence and XANES characterization of Ce⁴⁺ in
Ce³⁺, Mg²⁺-co-doped Gd₃Al₂Ga₃O₁₂ garnet crystals**

Géraldine Dantelle, Georges Boulon^{}, Yannick Guyot, Denis Testemale, Malgorzata Guzik,
Shunsuke Kurosawa, Kei Kamada, Akira Yoshikawa*

Dr. Géraldine Dantelle, Dr. Denis Testemale
Institut NEEL, CNRS/UGA UPR2940, 25 rue des Martyrs Grenoble, France and
ESRF, European Synchrotron Radiation Facility, 38042 Grenoble, France

Prof. Georges Boulon, Assoc. Prof. Yannick Guyot
Institut Lumière Matière (ILM), UMR5306 CNRS-UCB Lyon1, Université de Lyon, 69622
Villeurbanne, France
*georges.boulon@univ-lyon1.fr

Assoc. Prof. Malgorzata Guzik
Faculty of Chemistry, University of Wroclaw, ul. Joliot-Curie 14, 50-383 Wroclaw, Poland

Assoc. Prof. Shunsuke Kurosawa, Assoc. Prof. Kei Kamada, Prof. Akira Yoshikawa
Institute for Material Research (IMR), Tohoku University, 2-1-1 Katahira Aoba-ku, Sendai,
980-8577 Miyagi, Japan

Keywords : fast scintillator, Ce³⁺ and Ce⁴⁺ dopants, garnet crystals, optical spectroscopy,
XANES spectroscopy

Abstract

In this paper, the most advanced oxide scintillator Ce³⁺, Mg²⁺-co-doped Gd₃Al₂Ga₃O₁₂ (GAGG) garnet host, grown by using the Czochralski method at the Tohoku University, Sendai, is reported. The charge transfer absorption band in UV, like in other Ce³⁺, Mg²⁺-co-doped oxides, reveals the creation of stable Ce⁴⁺ oxidation state, in addition of the usual Ce³⁺ one, admitted as responsible of the scintillation mechanism improvement displayed by this garnet. Strangely, the confirmation of quantitative values of Ce⁴⁺ concentration has never been done and the goal is mainly focused on the presence of Ce⁴⁺ and the evaluation of the Ce³⁺/Ce⁴⁺ ratio measured by XANES spectroscopy at the Ce L_{III} threshold of the European Synchrotron Radiation Facility (ESRF). This result is compared with those obtained for Ce³⁺, Mg²⁺-co-doped LuAG and, also, in garnets without any Mg²⁺ ions like Ce³⁺-doped GAGG,

This article has been accepted for publication and undergone full peer review but has not been through the copyediting, typesetting, pagination and proofreading process, which may lead to differences between this version and the [Version of Record](#). Please cite this article as doi: [10.1002/pssb.201900510](https://doi.org/10.1002/pssb.201900510)

Ce³⁺-doped LuAG and Ce³⁺-doped YAG. The role of Li⁺ ion in place of Mg²⁺ one is also considered in Ce³⁺, Li⁺-co-doped LuAG single crystal.

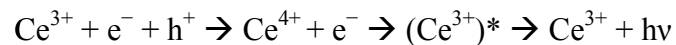
1. Introduction: state of the art of research on new fast garnet scintillators

Research on new fast inorganic scintillation crystals, is a critical pillar in the strategy of PET, a nuclear medicine imaging technique.^[1-3] Actually, the best scintillators used to convert high-energy radiation of the two gamma rays to UV-visible radiation are based of Ce³⁺ dopant in crystals, due to the parity-allowed electric dipole 5d-4f transitions which have larger oscillator strengths and shorter radiative lifetimes than the 4f-4f transitions of the trivalent rare earth ions. Selected scintillator crystals were Ce³⁺-doped orthosilicates as Gd₂SiO₅ (GSO), Lu₂SiO₅ (LSO), (Lu_{1-x}Y_x)₂SiO₅ (LYSO).^[4-7] As we always have to improve spatial and temporal performances of these scintillator crystals, great efforts are made to find new compounds like pyrosilicates based on RE₂Si₂O₇ (RE = Lu, Y, Gd), LaX₃ (X = Cl, Br) single crystal hosts.^[8-10] Also very important is research on garnet structure single crystals which are indeed promising candidates by combining high values of both density, stopping power for X-ray and γ -ray radiations and light yield. Well mastered crystal growth technology is deeply developed for doping by rare earth ions like Pr³⁺, Nd³⁺, Ho³⁺, Er³⁺, Tm³⁺, Yb³⁺ for lasers sources, Ce³⁺ for phosphors or Tb³⁺ for magneto-optic hosts. A remarkable scintillator-oriented combinatorial search in Ce³⁺-doped (Y,Gd)₃(Ga,Al)₅O₁₂ multi-component garnet compounds leads to find out new Ce³⁺-doped Gd₃Al₂Ga₃O₁₂ (GAGG) single crystals which have been demonstrated to be efficient exceeding the light yield values achieved for the best commercially used Ce³⁺-doped LYSO orthosilicate crystals.^[11-24] The research was also extended by Ce³⁺-doped garnet transparent ceramics of similar garnet compositions to single crystals which have displayed a more intense and faster scintillation signal than crystals.^[25-27]

2. Role of Ce⁴⁺ cations in the scintillation mechanism

In order to improve the time response properties and the light yield of several types of scintillators an approach has been made by codoping with divalent alkali earth elements such as Ca²⁺ and Mg²⁺ ions, changing the Ce³⁺ valence state into the Ce⁴⁺ one by the charge compensation mechanism which achieves charge neutrality.^[14, 18, 20, 21]

The presence of Ce⁴⁺ ions in Ce³⁺-doped materials has always been a big issue. The first precise work showing the presence of Ce⁴⁺ has been published in 1992 by Rotmann on Ce³⁺, Ca²⁺-co-doped YAG.^[28] Optically, it has been determined that the cerium can change valence state between Ce³⁺ and Ce⁴⁺ when annealed in an atmosphere of reducing and oxidizing gases, respectively. Under cathodoluminescence, the Ce³⁺ ion emission is seen even when only Ce⁴⁺ is present in the crystal and it was interpreted as an electron first entering a Ce⁴⁺ in an upper excited 5d state, thereby converting it temporarily to Ce³⁺, followed by the standard 5d→4f emission of Ce³⁺ at 550 nm. Then, in 2013, Blahuta & al. proposed, a new scintillation mechanism under ionizing irradiation involving Ce⁴⁺ ions in Ce³⁺-Mg²⁺/Ca²⁺-co-doped LYSO single crystals.^[7] Nowadays, in co-doped materials, the evidence of Ce⁴⁺ is admitted for the sequential charge capture of an electron-hole pair by Ce³⁺ according to:



Then, there is a continuous process of capturing a hole from the valency band.

As a result, Ce⁴⁺ ions are stabilized by the addition of Mg²⁺/Ca²⁺ divalent ions.^[14,18, 20, 21] Such centers create another fast radiative recombination pathway working in parallel with the classical mechanism based on the stable Ce³⁺ centers. It means the skipping of the first hole trapping stage could result in acceleration of the decay by suppression of slow components.^[29]

This observation has to be combined with the favorable position of the shallow levels below the conduction band leading to slow components of the decay. The main purpose of the Mg²⁺/Ca²⁺-co-dopant as analyzed by Melcher's group was to limit the formation of vacancies (Vo) that were detrimental in term of afterglow level.^[14,18] All previous results on Ce³⁺, Mg²⁺-co-doped GAGG are in favour of a promising scintillator for timing devices in high-energy physics and Time-of-Flight PET (TOF-PET) applications.

In this way, in the following part, we summarize the main spectroscopic properties of Ce³⁺-doped GAGG and Ce³⁺, Mg²⁺-co-doped GAGG garnet crystals.

3. Crystal growth and spectroscopic properties of Ce³⁺-doped Gd₃Al₂Ga₃O₁₂ (GAGG) and Ce³⁺, Mg²⁺-co-doped GAGG garnet crystals

Especially, the Ce³⁺-doped GAGG shown in **Figure 1a** and the Ce³⁺, Mg²⁺-co-doped GAGG shown in **Figure 1b** are single crystals developed by using the Czochralski method at IMR, Tohoku University.^[15, 21]

The absorption spectra of 0.5% Ce³⁺-doped GAGG and 0.5% Ce³⁺, 0.5% Mg²⁺-co-doped GAGG crystals are presented in **Figure 2**. We clearly see the two first Ce³⁺ 4f→5d absorption

bands at roughly 450 and 340 nm, respectively, the $Gd^{3+} 4f \ ^8S_{7/2} \rightarrow \ ^6P_J$ and $\ ^8S_{7/2} \rightarrow \ ^6I_J$ absorption lines and, especially in the co-doped crystal, the strong Ce^{4+} charge transfer band (CTB) in UV below 320 nm. This CTB is assigned from the oxygen 2p orbitals of the valence band to the $Ce^{4+} 4f$ orbitals by analogy with $Ce^{3+}, Mg^{2+}/Ca^{2+}$ -co-doped LYSO^[7] and also with Ce^{3+}, Mg^{2+} -co-doped $Lu_3Al_5O_{12}$ (LuAG) ceramics.^[26] The hole in the maximum of this broad absorption band at around 275 nm corresponds to the resonant energy transfer between the $Gd^{3+} \ ^6I_J \rightarrow \ ^8S_{7/2}$ emission lines and the Ce^{4+} CTB broad absorption which corresponds to a non-radiative energy transfer since Ce^{4+} centers do not emit. Finally, in Ce^{3+}, Mg^{2+} -co-doped GAGG there is two contributions to shortening of the decay: one due to the presence of Ce^{4+} and another one associated with the energy transfer from Gd^{3+} to Ce^{4+} ions. A discussion on the energy migration and energy transfer processes in the set of un-doped and Ce^{3+} activated multi-component garnet single crystals has been recently reported.^[30]

Radioluminescence spectra under excitation by X-rays from CuK α of the Ce^{3+} -doped GAGG and Ce^{3+}, Mg^{2+} co-doped GAGG are shown in **Figure 3**. The broad visible band is composed of the two usual transitions $5d \rightarrow 4f$ ($\ ^2F_{5/2}$) and $5d \rightarrow 4f$ ($\ ^2F_{7/2}$). It is important to mention the decreasing of the Ce^{3+} emission intensity by Mg^{2+} co-doping as a result of the creation of Ce^{4+} in these crystals and then the reduction of Ce^{3+} active centers.

Scintillation decays of the $5d \rightarrow 4f$ visible broad band of 1% Ce^{3+} -doped GAGG (0% Mg) and 1% $Ce^{3+}, 0.1\% Mg^{2+}$ co-doped GAGG crystals under excitation by ^{137}Cs radio-isotope (662 keV) are shown in **Figure 4**. Decay profiles can be fitted by two exponentials, corresponding to the fast and slow radiative recombination of the Ce^{3+} emitting centers. The decay-time components of 1% Ce^{3+} -doped GAGG (0% Mg) and 1% $Ce^{3+}, 0.1\% Mg^{2+}$ co-doped GAGG crystals and the corresponding percentage of the total scintillation output are listed in **Table 1**. The most prominent observation is the shortening of the scintillation decay-time after Mg^{2+} co-doping. Without Mg^{2+} , 1% Ce^{3+} -doped GAGG is characterized by 92.2 ns decay time (81%) and in 1% $Ce^{3+}, 0.1\% Mg^{2+}$ co-doped GAGG 58% of the total decay by 45.2 ns decay time. The shortening was already noticed first in $Ce^{3+}, Mg^{2+}/Ca^{2+}$ -co-doped LYSO crystal^[7], in Ce^{3+}, Ca^{2+} -co-doped GAGG crystal^[14] and Ce^{3+}, Mg^{2+} -co-doped LuAG ceramics.^[25-27]

Table 1 The decay-time components of 1% Ce³⁺-doped GAGG (0% Mg) and 1% Ce³⁺, 0.1% Mg²⁺ co-doped GAGG crystals and the corresponding percentage of the total scintillation output.

Samples	Light output %	Fast decay time (ns)/ ratio (%)	Slow decay time (ns)/ ratio (%)	Timing resolution/ps
0 % Mg	100	92.2/81	296/19	452
0.1% Mg (1000 at.ppm)	79	45.2/58	135/42	196
0.01% Mg (100 at.ppm)	93.5	39.6/53	132/47	

In Ce³⁺-doped Gd₃Al₂Ga₃O₁₂ single crystals, we should add the scintillation decays were accelerated by both Ca²⁺ and Mg²⁺ co-dopants. Comparing to Ca²⁺ co-doping, the Mg²⁺ co-doped samples showed much faster decay and comparatively smaller light output decrease with increasing Mg²⁺ dopant concentration but of enough intensity to be applied. The best sample corresponds to 100 at. ppm Mg²⁺ with performances mentioned in **Table1**.

Finally, Ce³⁺, Mg²⁺-co-doped GAGG shows improvement of both, shortening of the decay-time (45.2 ns on 58% of the decay), a fast timing resolution (196 ps, close to 180 ps, the value of the LYSO crystal) and a high light yield (44000 photon/MeV), corresponding to only 79% of the Ce³⁺-doped Gd₃Al₂Ga₃O₁₂ light output, so that is really a promising scintillator for application as positron emission tomography.

4. Evidence and evaluation of stable Ce⁴⁺ ions by XANES technique in Ce³⁺, Mg²⁺-co-doped GAGG

Previous articles considered that the charge transfer absorption band located at 260 nm is the probe of presence of Ce⁴⁺ ions in Ce³⁺, Mg²⁺/Ca²⁺-co-doped LYSO single crystals^[7] and Ce³⁺, Ca²⁺-co-doped GAGG^[6, 21]. This hypothesis seems in agreement with the creation of Ce⁴⁺ ions due to the introduction of divalent ions as Ca²⁺ and Mg²⁺. However, the quantitative values of the Ce³⁺/Ce⁴⁺ concentration ratio in Ce³⁺, Mg²⁺-co-doped GAGG have never been measured. Therefore, our goal is firstly focused on the confirmation of the

presence of Ce^{4+} ions in this crystal and secondly on the evaluation of the $\text{Ce}^{3+}/\text{Ce}^{4+}$ ratio measured by the X-ray Absorption Near Edge Spectroscopy (XANES) spectroscopy at the Ce L_{III} threshold which is another effective technique able to distinguish unambiguously the Ce^{3+} and Ce^{4+} oxidation states. Measurements have been made at the European Synchrotron Radiation Facility (ESRF) in Grenoble performed in high energy resolution fluorescence-detected (HERFD) mode at the Fame-UHD beamline. The photon energy was scanned from 5.68 keV to 5.85 keV using a Si (220) double-crystal monochromator. A glove box filled with helium was used between the samples, the crystal analyzer spectrometer and the detector, to avoid partial beam absorption by the air. The signal was recorded with a five-Ge (331) crystal analyzer and a Vortex-Ex detector. The beam size was $300 \times 100 \mu\text{m}^2$ (horizontal x vertical FWHM). The energy calibration was done using the CeO_2 spectrum. The $\text{Ce}^{3+}/\text{Ce}^{4+}$ ratio was determined by linear combination of XANES spectra of standards, *i.e.* nano- CeO_2 as a reference for Ce^{4+} and another Ce^{3+} -doped YAG single-crystal as a reference for Ce^{3+} [31]. The experimental data were analyzed using the *Demeter/Athena* software.[32] We also have evaluated the $\text{Ce}^{3+}/\text{Ce}^{4+}$ ratio by withdrawing ratio dependence of XANES spectra corresponding to different values of this ratio and compared with the experimental ones.

The Ce L_{III} threshold XANES spectra of $\text{Ce}(\text{acetate})_3$ and Ce^{3+} -doped YAG as Ce^{3+} trivalent reference (characteristic peak at 5727 eV) and CeO_2 as Ce^{4+} tetravalent reference (characteristic peak at 5738 eV) are shown in **Figure 5**. These two lines are enough dispersed to characterize each oxydation state. The XANES experimental data can be seen also for 0.5% Ce^{3+} -doped YAG, 0.5% Ce^{3+} -doped GAGG and 0.5% Ce^{3+} , 0.5% Mg^{2+} -co-doped GAGG garnet single-crystals in **Figure 6**, **Figure 7** and **Figure 8**, respectively. It is clear that we do not observe any signal from Ce^{4+} reference in 0.5% Ce^{3+} -doped YAG and 0.5% Ce^{3+} -doped GAGG and then, only the presence of Ce^{3+} ions is detected in these crystals without any Mg^{2+} , whereas in Ce^{3+} , Mg^{2+} -co-doped GAGG, Ce^{4+} ions are clearly observed. The estimation of the $\text{Ce}^{3+}/\text{Ce}^{4+}$ ratio in the spectra of 80/20 is the result of the linear combination fit method of the two Ce^{4+} and Ce^{3+} references. In **Figure 7** and **Figure 8**, we choose to draw the simulation of Ce^{4+} concentration dependences in order to show, at a glance, the evolution of the XANES spectra. The $\text{Ce}^{3+}/\text{Ce}^{4+}$ ratio of 82.5/17.5 mentioned in **Figure 8** for Ce^{3+} , Mg^{2+} -co-doped GAGG garnet single-crystal confirms the role of stable Ce^{4+} in the scintillation process and obviously the absence of stable Ce^{4+} in the crystals without any Mg^{2+} , as expected. Then, the two methods give the same order of magnitude of the $\text{Ce}^{3+}/\text{Ce}^{4+}$ ratio value, by considering an error of roughly 10% on the Ce^{4+} value.

It is worth mentioning an absolute quantitative estimation with XANES needs to know the absorption cross sections for both, the Ce^{3+} and Ce^{4+} transitions. If the $4f \rightarrow 5d$ electric dipole allowed transition cross section is known as high in different materials, the Ce^{4+} charge transfer absorption band is not known. However, a roughly comparison can be done from Figure 2 in Ce^{3+} , Mg^{2+} -co-doped GAGG garnet single-crystal when comparing the absorption areas of the first Ce^{3+} $4f \rightarrow 5d$ absorption band at 450 nm with the Ce^{4+} charge transfer absorption band in the 225-325 nm UV spectral range after deducing both Gd^{3+} absorption lines and the second Ce^{3+} $4f \rightarrow 5d$ absorption band at 340 nm. At a glance, areas shows values of the same order of magnitude giving some sense at the Ce^{3+}/Ce^{4+} ratio deduced from XANES spectra. In Ce^{3+} , Mg^{2+} -co-doped LYSO and Ce^{3+} , Ca^{2+} -co-doped LYSO⁷, the linear combination fit has been applied and provided 80/20 and 65/35 ratios, respectively, so that, with Mg^{2+} co-doping the same amounts of Ce^{4+} are observed in GAGG and LYSO. In 0.3% Ce^{3+} , 0,3% Mg^{2+} -co-doped LuAG transparent ceramics the Ce^{3+}/Ce^{4+} ratio is 75/25.^[26] The behaviour of Ce^{3+} , Ca^{2+} -co-doped GAGG garnet single crystal is completely different since the evaluated Ce^{3+}/Ce^{4+} ratio is 4/96.^[18]

The segregation coefficient of Ce^{3+} ions in garnets is far from one as we already analyzed it in melt crystal growth and ceramic processing for optical applications in YAG^[33-34] and $(Gd,Y)_3Al_5O_{12}$.^[35] Here, we started from the nominal concentrations of 1mol.% Ce^{3+} , 0.1 mol.% Mg^{2+} -co-doped GAGG. and we need to give some values of the real concentrations in the crystals. The solidification fraction (g) described as : $g = (\text{mass of grown crystal})/(\text{mass of starting materials in crucible})$ has been measured and was about 0.23. The composition distributions in grown crystals were monitored by the EPMA; JXA-8621MX, JEOL. The average effective segregation coefficient of Ce^{3+} is $K_{\text{eff}} = 0.23$. As a result, the real concentration of Ce^{3+} in the crystal is estimated between 0.15 and 0.38 mol.%.^[16] Traces of Mg^{2+} could not be detected by the EPMA but were analyzed by ICP-AES. Mg^{2+} concentration at $g = 0.1$ and $g = 0.2$ were 16 and 25 wt. ppm (0.061 and 0.091 mol%), respectively.

Indeed, we have always to take into account of the competition for scintillation mechanisms between the creation of Ce^{4+} and the presence of the shallow electron traps and deeper traps in the crystal lattice of garnet. These traps capture electrons from the conduction band and contribute to extend component in scintillation decay. It is difficult at this point to evaluate each contribution of Ce^{4+} ion and traps to the fastest component of scintillation response. It is only clear that Ce^{3+} , Mg^{2+} -co-doped GAGG shows lower afterglow and

thermo-stimulated luminescence intensity^[22] and there is an improvement of fast performances from the creation of Ce⁴⁺.^[20]

5. XANES data with Ce³⁺-doped LuAG, Ce³⁺, Li⁺-co-doped LuAG and Ce³⁺, Mg²⁺-co-doped LuAG

Ce³⁺-activated LuAG single-crystal is another extensively studied fast and bright scintillator which is demanded in coming medical and industrial applications. Especially, the development of Ce³⁺-doped Lu₃Al₅O₁₂ (LuAG)-based single crystal scintillators is a good example of materials prepared by the micro-pulling down method at the initial stage of material screening and by Czochralski or Bridgman methods to obtain higher quality and larger size single crystals afterward.^[23] It has been observed that these materials gave rise to new class of ultra-efficient complex oxide scintillators, the light yield of which considerably exceeds the values achieved for the best Ce³⁺-doped orthosilicate scintillators. The interpretation is rather based on trapping processes including the nature and role of material defects giving rise to shallow traps at small energies below the conduction band and Ce⁴⁺ is not referred. Then, the Ce³⁺, Li⁺ co-doped Lu₃Al₅O₁₂ single crystals were also prepared by micro pulling down method and, namely the scintillation decay and light yield have revealed the effect of the co-doping like the smooth Ce⁴⁺ charge transfer absorption below 350 nm which is clearly enhanced with increasing concentration of Li⁺.^[24] Again, the scintillation decays were accelerated and light yields were increased by Li⁺ co-doping. In Ce³⁺, Ca²⁺/Mg²⁺/Li⁺-co-doped LuAG crystals and ceramics, interesting similarities have been found with the previous analysis of Ce³⁺, Ca²⁺/Mg²⁺-co-doped GAGG, mainly by the role demonstrated of Ce⁴⁺ ions.^[25-27] Consequently, it is worthwhile finding out what makes these materials unique and what they all have in common.

Single crystals have been grown also at IMR, Tohoku University, and co-doped not only with Mg²⁺ but also with Li⁺ ions, with the objective to compare results to those of the above GAGG crystals. As for segregation phenomenon, measurements have been done only for Ce³⁺, Li⁺-co-doped GAGG but not for Ce³⁺, Li⁺-co-doped LuAG. From the nominal concentration 0.15mol.% Li⁺, 1mol.% Ce³⁺ -co-doped GAGG we have found the average effective segregation coefficient K_{eff} of Ce³⁺, Ga³⁺ and Al³⁺ ions showed $K_{\text{eff}} = 0.28, 0.94$ and 1.06 values respectively. The composition distributions in grown crystals were monitored by the EPMA. Trace of Li could not be detected by the EPMA. Li concentration was analyzed by the glow discharge mass spectrometry (GD-MS). Li concentration at $g = 0.1$ and $g = 0.25$

were 5.1 and 3.2 wt ppm (0.023 and 0.014 mol%), respectively. Li concentration was decreased with increasing solidification fraction. This indicates evaporation of Li oxide during the crystal growth. Then, the real composition was 0.023-0.014 mol.% Li^+ , Ce 0.25-0.5 mol.% Ce^{3+} -co-doped GAGG. We can only say that the real concentration with respect of the nominal concentration in LuAG may vary in the same way as for GAGG due to the same conditions of crystal growths.

The Ce_{LIII} -edge XANES spectra of 0.5% Ce^{3+} -doped LuAG, 0.5% Ce^{3+} , 0.5% Li^+ -co-doped LuAG and 0.5% Ce^{3+} , 0.3% Mg^{2+} -co-doped LuAG shown in **Figure 9** are the first spectra ever recorded for these crystals. First, we note it make sense that Ce^{3+} -doped LuAG does not contain any trace of Ce^{4+} , as well non-co-doped Ce^{3+} -doped YAG and Ce^{3+} -doped GAGG. Only Ce^{3+} , Mg^{2+} -co-doped LuAG shows a weak noisy signal at 5738 eV and then shows the presence of traces of Ce^{4+} ion consistently with Ce^{3+} , Mg^{2+} -co-doped GAGG. To confirm this Ce^{4+} signal, let's remind Nikl & al¹⁹ have reported the Ce^{4+} charge transfer absorption band clearly observed and enhanced with increasing concentration of Mg^{2+} codopant. We have also compared the XANES spectrum with the weak XANES spectra analysed in Ce^{3+} , Mg^{2+} -co-doped LuAG transparent ceramic^[26]. It makes sense to compare the results of both, crystal (0.5% Mg^{2+}) and transparent ceramics (0.3% Mg^{2+} corresponding to the maximum of light output at 25070 ph/MeV). The Ce^{4+} concentration of 25% has been evaluated in this transparent ceramics and clearly increased to 37% of Ce^{4+} ion when the Mg^{2+} concentration was increased from 0.3% to 0.6%. As a result, we can conclude that Ce^{4+} ion plays the same role with the same concentrations in scintillation mechanisms of Ce^{3+} , Mg^{2+} -co-doped LuAG garnet, either for crystal or for transparent ceramics.

On the other hand, a major feature has to be mentioned: XANES spectra does not show any trace of Ce^{4+} in Ce^{3+} , Li^+ -co-doped LuAG. It means, although interesting scintillation data have been reported, the real role of Ce^{4+} remains questionable^[23-24]. As an example, an increase of the absorption below 350 nm that could be related to formation of Ce^{4+} oxidation state has been recorded in Ce^{3+} , Li^+ -co-doped LuAG grown by micro-pulling and compared to Ce^{3+} -doped LuAG, the scintillation decay was accelerated and the high light yield of 24,000 photon/MeV was obtained with 0.2% Li (200 ppm) co-doped samples.^[31] It has been suggested that Li^+ ions in Ce^{3+} , Li^+ -co-doped LuAG do substitute Lu^{3+} sites with charge balance attained in part by conversion of Ce^{3+} to Ce^{4+} and creation of O⁻ hole centers, whereas in Ce^{3+} , Li^+ -co-doped YAG, Li^+ goes in interstitial position with charge compensation attained by reduction of anion vacancies.^[22,29] The behaviour of these Lu-based

garnet scintillators is then different from other Y or Gd-based garnets and should be more deeply analysed. The absence of detectable Ce^{4+} ion from these XANES spectra, as compared with those of Ce^{3+} , Mg^{2+} -co-doped GAGG and Ce^{3+} , Mg^{2+} -co-doped LuAG, induces some questions on the scintillation mechanism in Ce^{3+} , Li^+ -co-doped LuAG.

6. Conclusion

In this work, we were dealing with the most advanced oxide scintillator Ce^{3+} , Mg^{2+} -co-doped $Gd_3Al_2Ga_3O_{12}$ (GAGG) garnet host, grown at the Tohoku University, Sendai, for applications which require fast timing resolution and high light yield such as PET. The co-doping of Ce^{3+} ion by Mg^{2+} one has revealed the creation of Ce^{4+} ion, assigned from the charge transfer absorption band in UV, due to charge compensation effect, occurring in the scintillation mechanisms, in addition of the usual Ce^{3+} ion, like in Ce^{3+} , Ca^{2+} -co-doped GAGG and Ce^{3+} , Mg^{2+} -co-doped LYSO oxydes. The presence and then the role played by the stable Ce^{4+} ion in this garnet for the scintillation mechanisms has been demonstrated by XANES spectroscopy at the Ce L_{III} threshold of the European Synchrotron Radiation Facility (ESRF) in Grenoble. In addition, the estimation of the Ce^{3+}/Ce^{4+} ratio measured by a linear combination fit method is 80/20 and 82.5/17.5 from the simulation of Ce^{4+} curves.

XANES analysis also reveals the creation of Ce^{4+} in Ce^{3+} , Mg^{2+} -co-doped LuAG crystal, another important scintillator, like it was shown in transparent ceramics of the same composition and confirms the absence of stable Ce^{4+} in crystals like Ce^{3+} -doped GAGG, Ce^{3+} -doped LuAG and Ce^{3+} -doped YAG, respectively, without any Mg^{2+} ion. It means that the scintillation mechanisms are probably the same in Ce^{3+} , Mg^{2+} -co-doped GAGG and Ce^{3+} , Mg^{2+} -co-doped LuAG garnet crystals with the occurrence of stable Ce^{4+} ion. On the other side, any trace of Ce^{4+} ion has not been detected in Ce^{3+} , Li^+ -co-doped LuAG, in which Mg^{2+} has been substituted by Li^+ . Nevertheless, this crystal is considered as efficient for scintillation. Despite some discussion in literature on the nature of luminescence centers, the real mechanisms of scintillation with Li^+ ions have to be more clearly understood.

References

- [1] M. Balcerzyk, Z. Gontarz, M. Moszynski, M. Kapusta, *J. Lumin.* **2000**, 87, 963.
- [2] M. Conti, *Phys. Med.* **2009**, 25, 1.
- [3] M. Nikl, A. Yoshikawa, *Adv. Opt. Mater.* **2015**, 3(4), 463.
- [4] C. L. Melcher and J. S. Schweitzer, *IEEE Trans. Nucl. Sci.* **1992**, 39, 502.
- [5] M. Kapusta, P. Szupryczynski, C. L. Melcher, M. Moszynski, M. Balcerzyk, and A. A. Carey, *IEEE Trans. Nucl. Sci.* **2005**, 52(4), 1098.

- [6] M. A. Spurrier, P. Szupryczynski, A. A. Carey, and C. L. Melcher, *IEEE Trans. Nucl. Sci.* **2008**, *55*(3), 1178.
- [7] S. Blahuta, A. Bessi re, B. Viana, P. Dorenbos, and V. Ouspenski, *IEEE Trans. Nucl. Sci.* **2013**, *60*, 3134.
- [8] K. S. Shah, J. Glodo, M. Klugerman, W. W. Moses, S. E. Derenzo, and M. J. Weber, *IEEE Trans. Nucl. Sci.* **2003**, *50*(6), 2410.
- [9] K. W. Kramer, P. Dorenbos, H. U. Gudel, and C. W. E. van Eijk, *J. Mater. Chem.* **2006**, *16*, 2773.
- [10] M. S. Alekhin, *Appl. Phys. Lett.* **2014**, *104*, 161915.
- [11] K. Kamada, T. Yanagida, J. Pejchal, M. Nikl, T. Endo, K. Tsutumi, Y. Fujimoto, A. Fukabori and A. Yoshikawa, *J. Phys. D: Appl. Phys.* **2011**, *44*(50), 505104.
- [12] K. Kamada, T. Endo, K. Tsutumi, T. Yanagida, Y. Fujimoto, A. Fukabori, Y. Yoshikawa, *Cryst. Growth Des.* **2011**, *11*, 4484.
- [13] K. Kamada, T. Yanagida, T. Endo, K. Tsutumi, Y. Usuki, and M. Nikl, *J. Cryst. Growth* **2012**, *352*, 88.
- [14] M. Tyagi, F. Meng, M. Koschan, S. B. Donald, H. Rothfuss, C. L. Melcher, *J. Phys. D, Appl. Phys.* **2013**, *46*, 475302.
- [15] K. Kamada, S. Kurosawa, P. Prusa, M. Nikl, V. Kochurikhin, T. Endo, K. Tsutumi, H. Sato, Y. Yokota, K. Sugiyama, A. Yoshikawa, *Opt. Mater.* **2014**, *36*, 1942.
- [16] K. Kamada, Y. Shoji, V. Kochurikhin, A. Nagura, S. Okumura, S. Yamamoto, J. Yeom, S. Kurosawa, J. Pejchal, Y. Yokota, Y. Ohashi, M. Nikl, M. Yoshino, A. Yoshikawa *IEEE Trans. Nucl. Sci.* **2016**, *63*(2), 443.
- [17] J. Yeom, S. Yamamoto, S. E. Derenzo, V. Ch. Spanoudaki, K. Kamada, T. Endo, C. S. Levin, *IEEE Trans. Nucl. Sci.* **2013**, *60*(2), 988.
- [18] Y. Wu, F. Meng, Q. Li, M. Koschan, C. L. Melcher, *Phys. Rev. Appl.* **2014**, *2*, 044009.
- [19] M. Nikl, K. Kamada, V. Babin, J. Pejchal, K. Pilarova, E. Mihokova, A. Beitlerova, K. Bartosiewicz, S. Kurosawa, and A. Yoshikawa, *Cryst. Growth Des.* **2014**, *14*, 4827.
- [20] K. Kamada, M. Nikl, S. Kurosawa, A. Beitlerova, A. Nagura, Y. Shoji, J. Pejchal, Y. Ohashi, Y. Yokota, A. Yoshikawa, *Opt. Mater.* **2015**, *41*, 63.
- [21] K. Kamada, Y. Shoji, V. Kochurikhin, A. Nagura, S. Okumura, S. Yamamoto, J. Yeom, S. Kurosawa, J. Pejchal, Y. Yokota, Y. Ohashi, M. Nikl, M. Yoshino, A. Yoshikawa, *IEEE Trans. Nucl. Sci.* **2016**, *63*(2), 443.
- [22] W. Chewpraditkul, N. Pattanaboonmee, O. Sakthong, K. Wantong, W. Chewpraditkul, A. Yoshikawa, K. Kamada, S. Kurosawa, T. Szczesniak, M. Moszynski, V. Babin, M. Nikl,

Opt. Mater. **2019**, *92*, 181.

[23] M. Nikl, A. Yoshikawa, K. Kamada, K. Nejezchleb, C.R. Stanek, J.A. Mares, K. Blazek, *Prog. Cryst. Growth Charact. Mater.* **2013**, *59*, 47.

[24] K. Kamada, M. Nikl, S. Kurosawa, A. Beitlerova, A. Nagura, Y. Shoji, J. Pejchal, Y. Ohashi, Y. Yokota and A. Yoshikawa, *J. Cryst. Growth* **2016**, *452*, 85.

[25] S. Liu, X. Feng, Z. Zhou, M. Nikl, Y. Shi, and Y. Pan, *Phys. Status Solidi RRL*, **2014**, *8(1)*, 105.

[26] S. Liu, J. A. Mares, X. Feng, A. Vedda, M. Fasoli, Y. Shi, H. Kou, A. Beitlerova, L. Wu, C. D'Ambrosio, Y. Pan, M. Nikl, *Adv. Opt. Mater.* **2016**, *4*, 731.

[27] J. Li, S. Sahi, M. Groza, Y. Pan, A. Burger, R. Kenarangui, W. Chen, *J. Am. Ceram. Soc.* **2017**, *100*, 150.

[28] S. R. Rotman, H. L. Tuller, and C. Warde, *J. Appl. Phys.* **1992**, *71*, 1209.

[29] M. V. Derdzyan, K. L. Hovhannesian, A. V. Yeganyan, R. V. Sargsyan, A. Novikov, A. G. Petrosyan, C. Dujardin, *Cryst. Eng. Comm.* **2018**, *20*, 1520.

[30] K. Bartosiewicz, V. Babin, K. Kamada, A. Yoshikawa, M. Nikl, *J. Lum.* **2015**, *166*, 117.

[31] M. Tella, M. Auffan, L. Brousset, E. Morel, O. Proux, C. Chanéac, B. Angeletti, C. Pailles, E. Artells, C. Santaella, J. Rose, A. Thiéry, J.-Y. Bottero, *Environ. Sci.: Nano*, **2015**, *2*, 653.

[32] <https://bruceravel.github.io/demeter/>

[33] V. Chani, G. Boulon, W. Zhao, T. Yanagida, A. Yoshikawa, *Jpn. J. App. Phys.* **2010**, *49* 075601.

[34] W. Zhao, S. Anghel, C. Mancini, D. Amans, G. Boulon, T. Epicier, Y. Shi, X.Q. Feng, Y.B. Pan, V. Chani, A. Yoshikawa, *Opt. Mater.* **2011**, *33*, 684–687.

[35] W. Zhao, C. Mancini, D. Amans, G. Boulon, T. Epicier, Y. Min, H. Hideki, T. Yanagitani, T. Yanagida, A. Yoshikawa, *Jpn. J. App. Phys.* **2010**, *49* 022602.

FIGURES

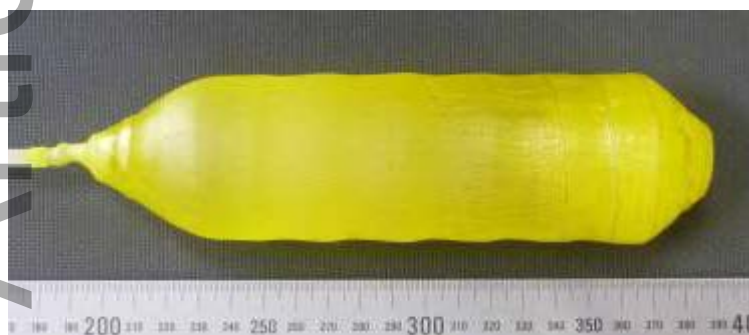


Figure 1a Garnet single crystal: 2 inch size 1%Ce³⁺-doped Gd₃Al₂Ga₃O₁₂ (GAGG) garnet single crystal grown by the CZ method at IMR, Tohoku University, Sendai, Japan.

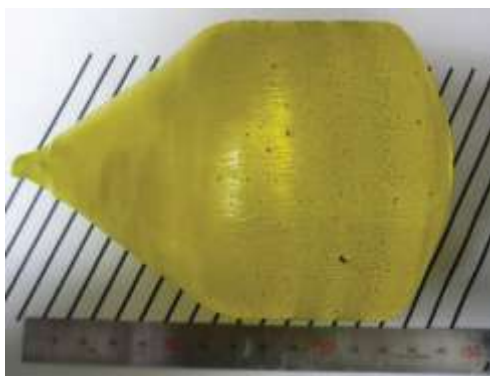


Figure 1b Garnet single crystal: 3 inch diameter of 1%Ce, 0.1%Mg-co-doped Gd₃Al₂Ga₃O₁₂ (GAGG) garnet single crystal grown by the CZ method at IMR, Tohoku University, Sendai, Japan.

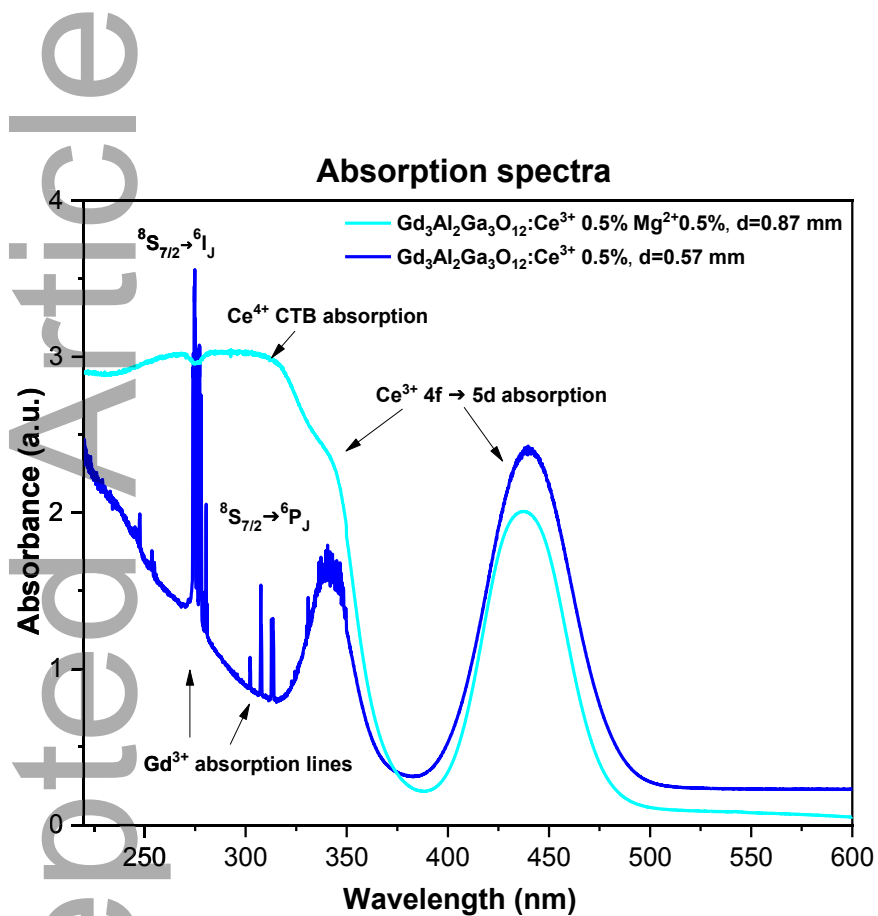


Figure 2 Absorption spectra at room temperature of the 0.5% Ce^{3+} -doped GAGG and 0.5% Mg^{2+} , 0.5% Ce^{3+} -co-doped GAGG crystals, at room temperature.

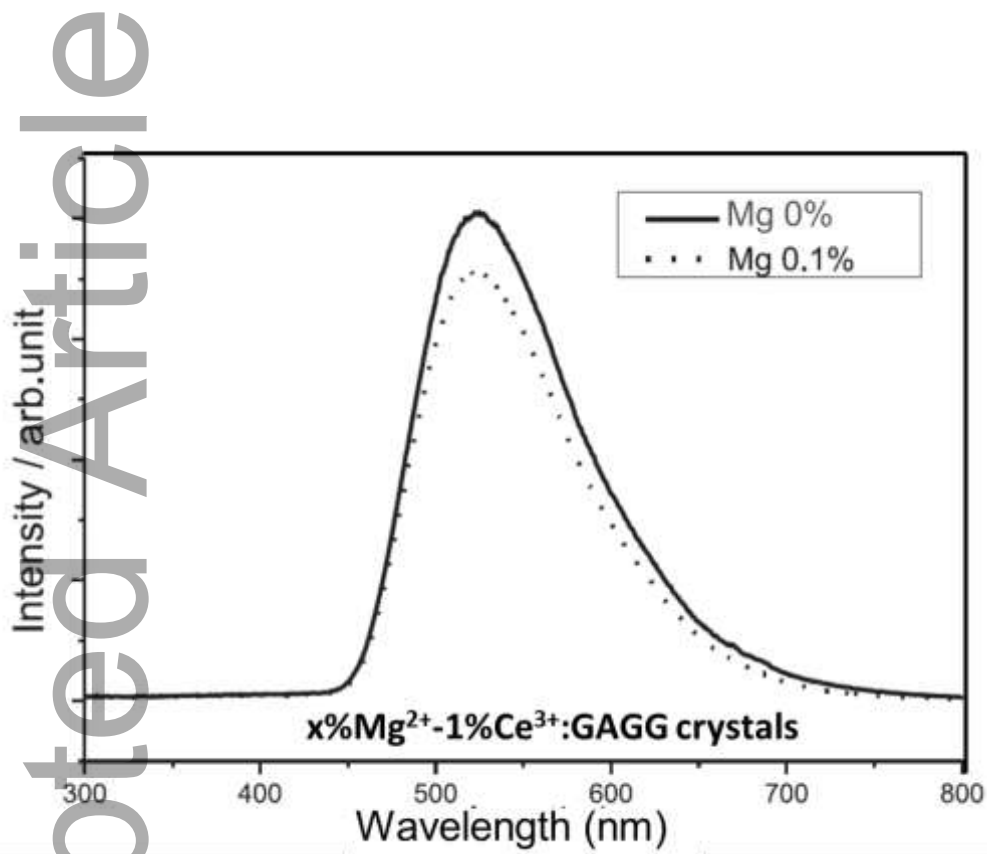


Figure 3 Radioluminescence spectra at room temperature of the $5d \rightarrow 4f$ transition of Ce^{3+} in 1% Ce^{3+} :GAGG and 0.1% Mg^{2+} , 1% Ce^{3+} -co-doped GAGG crystals. Excitation by X-rays, CuK α , 40 kV, 30 mA.

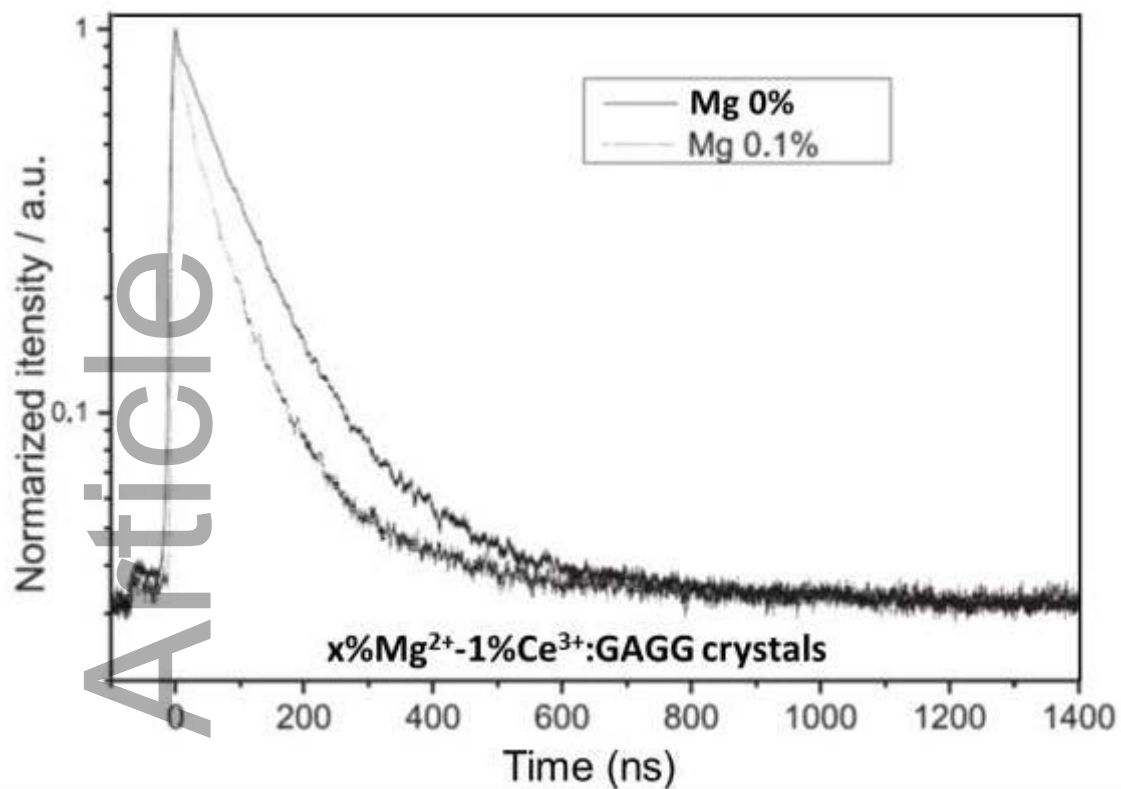


Figure 4 Scintillation decay profiles at room temperature of the 5d→4f visible broad band of the 1%Ce³⁺-doped GAGG (0% Mg²⁺) and 1%Ce³⁺, 0.1%Mg²⁺-co-doped GAGG crystals under excitation by ¹³⁷Cs radio-isotope (662 keV).

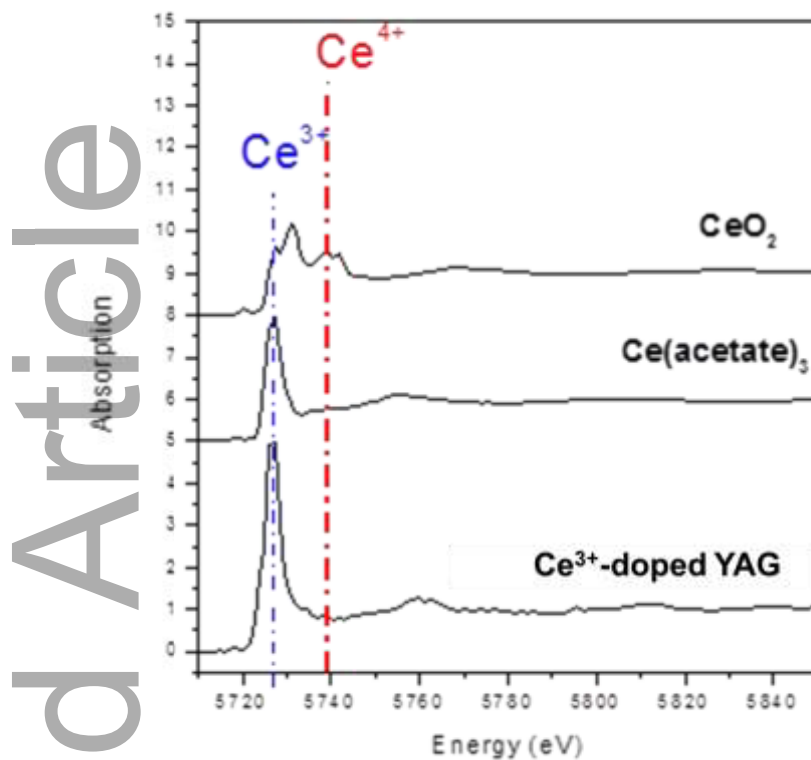


Figure 5 The XANES spectroscopy at the Ce L_{III} threshold. X-ray absorption spectra of Ce³⁺ and Ce⁴⁺ are different. CeO₂ is chosen as a reference for Ce⁴⁺ (characteristic peak at 5738 eV) and Ce(acetate)₃ and Ce³⁺-doped YAG are chosen as a reference for Ce³⁺ (characteristic peak at 5727 eV).

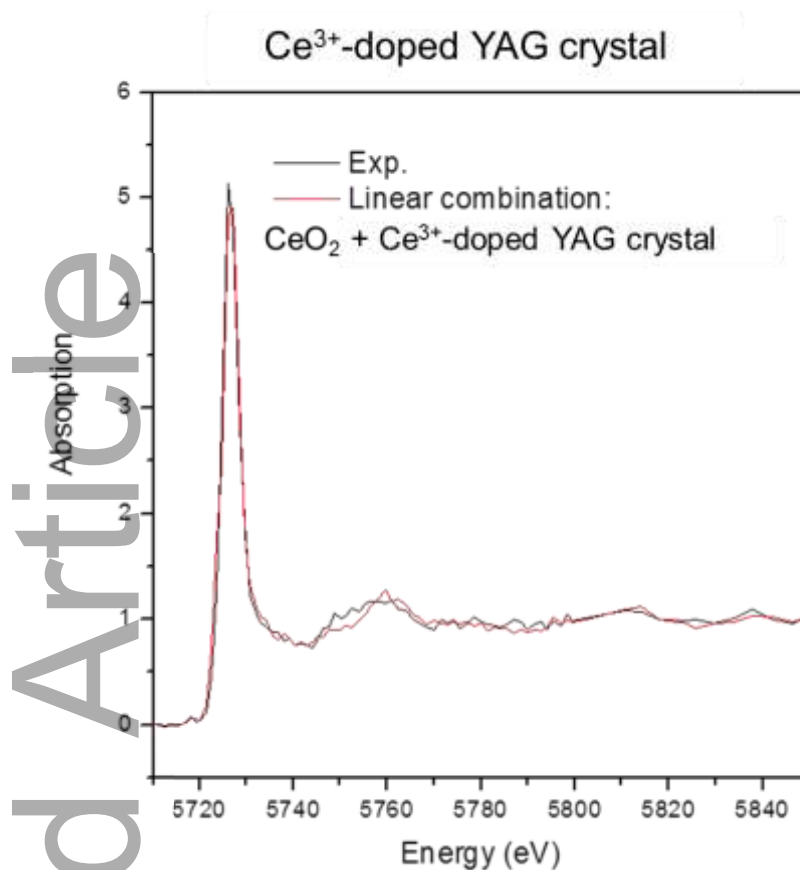


Figure 6 Comparison of the experimental XANES spectrum of the 0.5% Ce³⁺-doped YAG single-crystal (black, with thickness=0,53mm) with the spectrum obtained by a linear combination fit method. Another Ce³⁺-doped single-crystal is used as a reference for Ce³⁺ (red). We observe the presence of only Ce³⁺ ions in this sample.

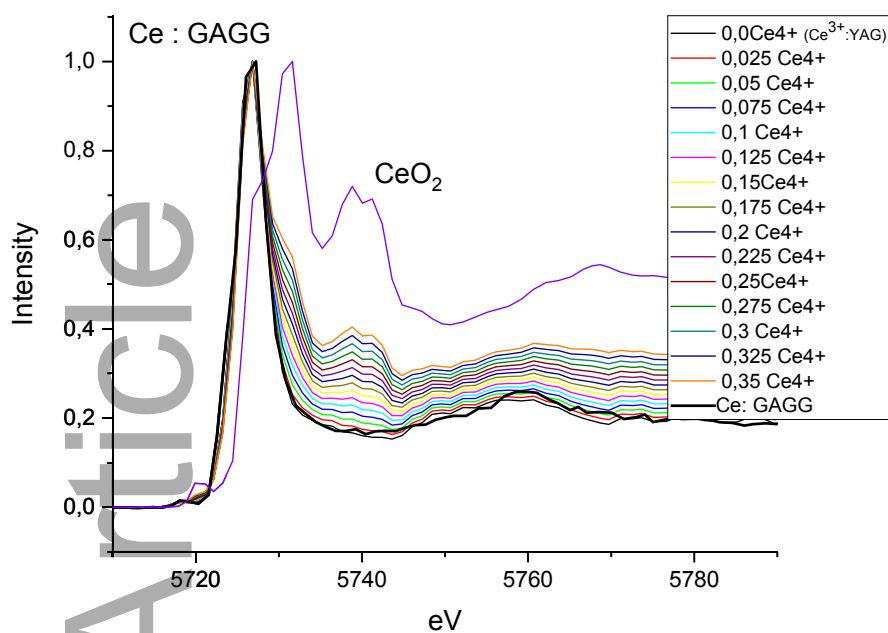


Figure 7 Experimental Ce L_{III}-edge XANES spectra of Ce³⁺-doped GAGG garnet single crystal (black curve). The XANES spectra of the Ce⁴⁺ (CeO₂) and Ce³⁺ (Ce³⁺: YAG) mentioned here by 0.0 Ce⁴⁺, are used as references. Ratio dependence of XANES spectra have been simulated for different Ce⁴⁺ concentrations. Any trace of Ce⁴⁺ has been detected and so the sample contains only Ce³⁺.

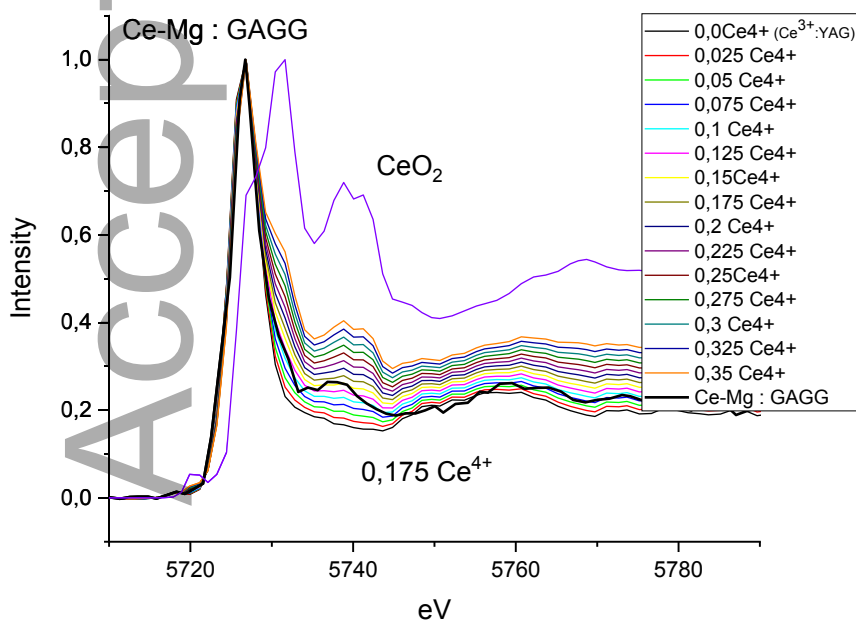


Figure 8 Experimental Ce L_{III} -edge XANES spectra of Ce^{3+} , Mg^{2+} -co-doped GAGG garnet single crystal (black curve). The XANES spectra of the Ce^{4+} (CeO_2) (violet) and Ce^{3+} (Ce^{3+} :YAG) mentioned here by 0.0 Ce^{4+} (black), are used as references. Ratio dependence of XANES spectra have been simulated for different Ce^{4+} concentrations. The sample contains 17.5% Ce^{4+} and then 82.5% Ce^{3+} .

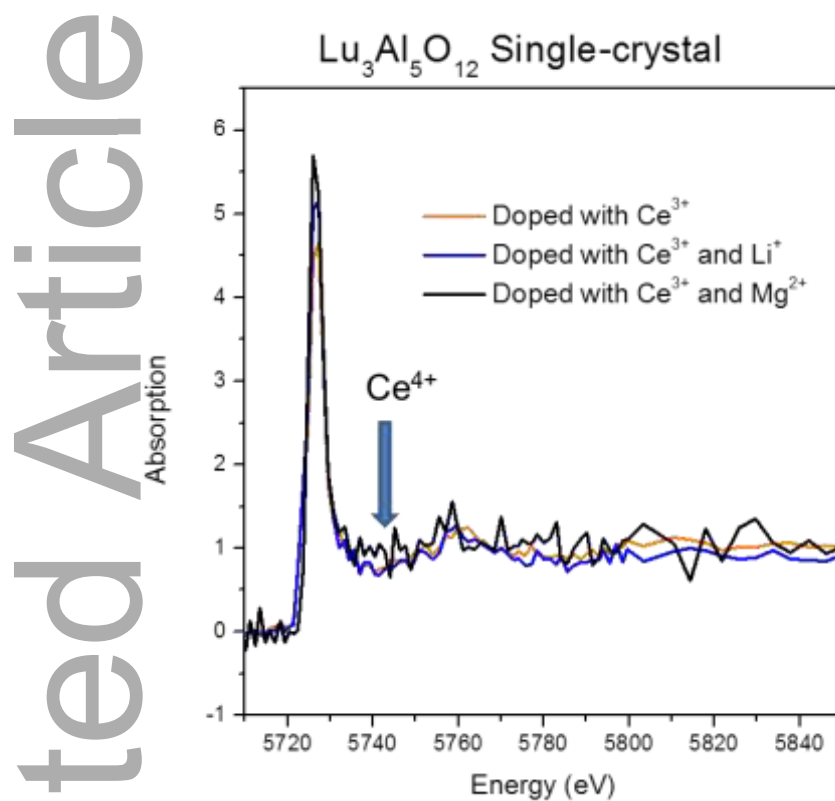
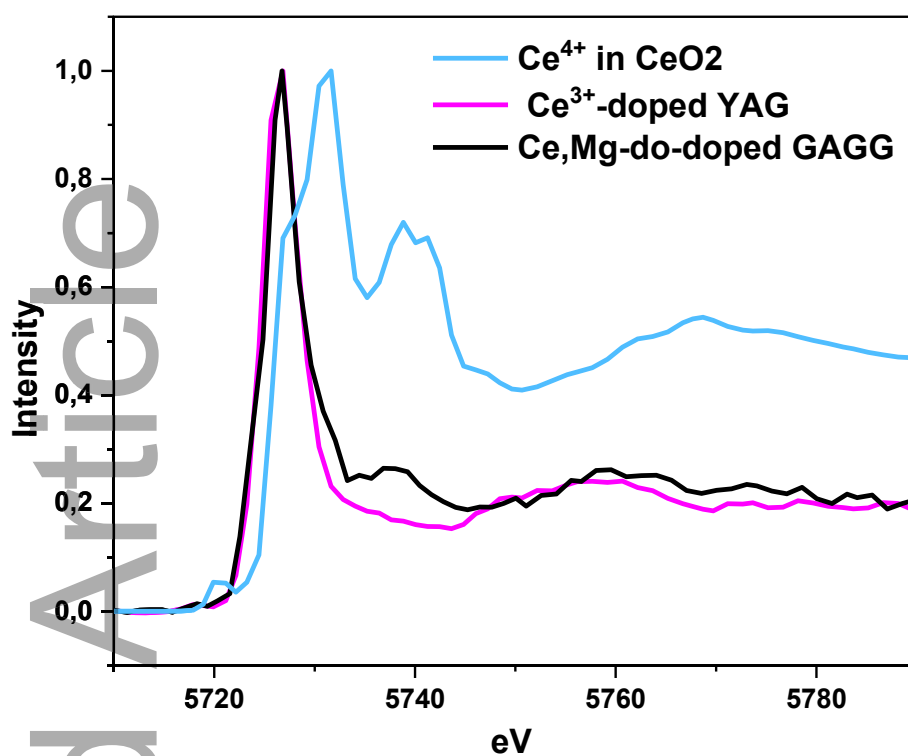


Figure 9 Experimental Ce L_{III} -edge XANES spectra of Ce^{3+} -doped LuAG (red), Ce^{3+} , Li^+ -co-doped LuAG (blue) and Ce^{3+} , Mg^{2+} -co-doped LuAG (black), respectively. Only Ce^{3+} , Mg^{2+} -co-doped LuAG shows a weak noisy signal at 5738 eV and then the presence of Ce^{4+} ion. Thickness of samples=0,53mm.



Normalized experimental Ce L_{III}-edge XANES spectra of 1%Ce³⁺, 0.1%Mg²⁺-co-doped GAGG garnet single crystal (black curve). The normalized XANES spectra of the Ce⁴⁺ ion in CeO₂ (blue curve) and Ce³⁺-doped YAG (pink curve) are used as references. 0.175%Ce⁴⁺ and 0.825% Ce³⁺ have been detected.